Pergamon

Int. J. Solids Structures Vol. 33, No. 20–22, pp. 3215–3237, 1996

0020–7683/96 $15.00 + .00

0020–7683(95)00246–4

LARGE ELASTO-PLASTIC FINITE ELEMENT ANALYSIS OF SOLIDS AND SHELLS WITH THE ENHANCED ASSUMED STRAIN CONCEPT

DEANE ROEHL
Department of Civil Engineering, Catholic University of Rio de Janeiro, Brazil

and

EKKEHARD RAMM
Institute for Structural Analysis, University of Stuttgart, Germany

Abstract—A finite element simulation of arbitrarily large elasto-plastic deformations of three-dimensional and shell structures is described. Two numerical aspects originally developed by J. C. Simo have been combined, i.e. the multiplicative large strain plasticity and the enhanced assumed strain finite element concept. The constitutive model is worked out in its algorithmic version applying projection methods and consistent linearization. The enhanced strain field is added to the conventional hexahedral displacement elements avoiding volumetric locking in the plastic range. In addition to solid structures, the three-dimensional material model without any modifications is also applied to thin-walled shell structures. Here an extended shell formulation, a so-called seven-parameter model, is used in which the thickness strain is augmented by a linear term. The applicability of the entire formulation is demonstrated by several numerical examples. Copyright © 1996 Elsevier Science Ltd.

1. OBJECTIVE

The objectives of the present study can be summarized as follows:

—to handle arbitrarily large deformations (displacements and strains) in a three-dimensional setting,
—to apply a phenomenological, structure oriented material formulation for ductile materials with small elastic but large plastic deformations which is mechanically and numerically consistent,
—to use a finite element discretization free of any kind of locking or numerical instability,
—to apply the same three-dimensional material model without any manipulations, i.e. as it is, to a special three-dimensional oriented shell formulation.

In order to satisfy these objectives two of the many brilliant achievements of J. C. Simo have been adopted: the first one is his stringent development of the multiplicative large strain elasto-plasticity (Simo, 1988a; 1988b) applying also the principle of the maximum plastic dissipation. The consequent use of a spatial description with convective coordinates makes the formulation mechanically elegant; however, its success is primarily caused by a strict application of the return-mapping schemes and the derivation of a consistent algorithmic material tangent previously developed for classical small strain plasticity (Simo and Taylor, 1985).

The second idea refers to the finite element discretization. In order to avoid the well known deficiencies of pure displacement models Simo and Rifai (1990) introduced the so-called Enhanced Assumed Strain (EAS)-concept. The displacement dependent strain field of a standard displacement model is enhanced by an incompatible, i.e. element referred, extra strain field. The formulation leads to a typical hybrid–mixed element which easily allows resortion to a strain-driven material formulation. As shown in Simo and Rifai (1990) the EAS-concept can be derived from a three-field Hu–Washizu functional which condenses

to a two-field variational principle if certain conditions on the extra strain field are satisfied and an independent stress field drops out. It should be noted that due to these properties the consistent stress recovery is still a matter of discussion. Also it has been recently recognized that EAS-elements may show zero-energy modes during loading, so that certain stabilization schemes have to be introduced.

In this study, the standard brick element, e.g. the trilinear hexahedral displacement element with eight nodes, is enhanced by either three or six extra strain parameters. It is shown that not only the pathological volumetric locking in the incompressible limit can be avoided, but also localization can be captured by these elements.

Thin-walled structures, like plates and shells, usually resort to a reduced set of the full stress/strain space. For example, the normal stress/strain components in the thickness direction are set to zero. For material modelling even the assumption of a plane stress condition is quite common. This, in turn, requires a reduction of the constitutive law which for general material laws is not explicitly possible or leads to elaborate expressions. Therefore, one main objective is to allow the application of a non-reduced full set of constitutive equations. This means that the shell formulation also needs an extension so that all stress/strain components are included. A related shell model has been developed in Büchter and Ramm (1992) and Büchter *et al.* (1994), and is applied in this study, i.e. the three-dimensional material law used for bricks can also be directly inserted into the shell formulation. This so-called seven-parameter model adds to the three displacements of the reference surface and the three relative displacement components of the outside surfaces a linear transverse normal strain as an extra variable to avoid a "thickness locking". This additional variable is again introduced on the element level via the EAS-concept.

The paper is organized as follows. First, the constitutive model for large strain elasto-plasticity is described. The discretization in the context of the EAS-concept follows. Finally, its application to three-dimensional and shell problems is shown.

2. CONSTITUTIVE FRAMEWORK

The spatial deformation of an arbitrary body is shown in Fig. 1 which also includes the basic notation of the motion. The framework for finite strain elasto-plasticity which follows is based on the multiplicative decomposition of the deformation gradient, as for example proposed by Lee (1969).

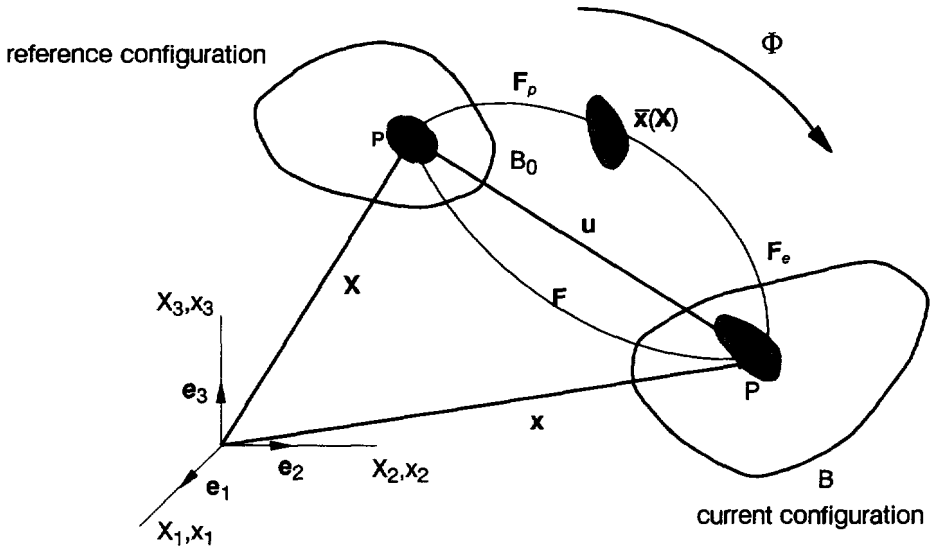

Fig. 1. Kinematics of the deformation.

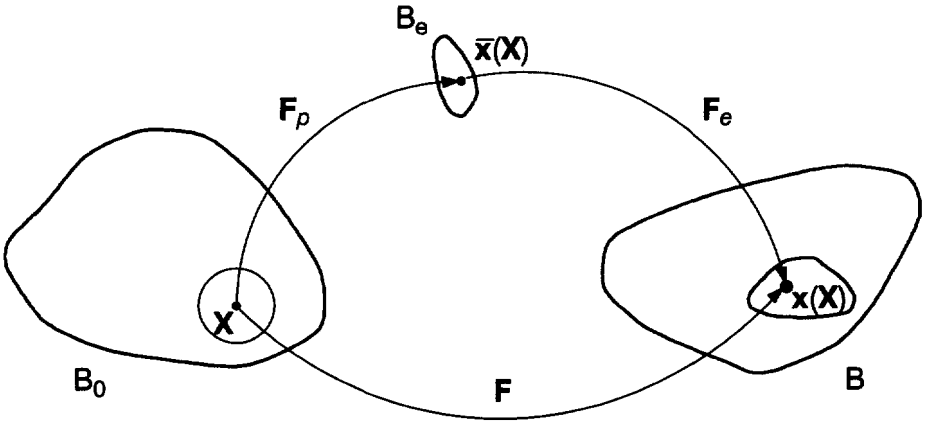

Fig. 2. Reference, current and intermediate configurations.

$$\mathbf{F} = \mathbf{F}_e \mathbf{F}_p. \tag{1}$$

The notion of an unstressed incompatible intermediate configuration which is up to a rotation uniquely defined, is associated with this decomposition (Fig. 2). We assume that a local rotation of the intermediate configuration does not affect the elastic response which is justified for isotropic materials with isotropic hardening laws.

Further, we assume the existence of a strain energy function W which is for the special case of isotropy a symmetric scalar function of the invariants of the deformation tensor. In a spatial description it follows with ϱ being the density:

$$W(\mathbf{F}) = \varrho\Psi = \tilde{W}(J_1(\mathbf{b}), J_2(\mathbf{b}), J_3(\mathbf{b})). \tag{2}$$

The hyperelastic constitutive relation between the Kirchhoff stress tensor τ and the elastic left-Cauchy–Green deformation tensor $\mathbf{b}$ is then

$$\tau = 2\varrho_0 \frac{\partial \Psi}{\partial \mathbf{g}} = 2\varrho_0 \mathbf{b} \frac{\partial \Psi}{\partial \mathbf{b}}. \tag{3}$$

The covariant metric tensor is denoted by $\mathbf{g}$.

Additionally, an elasto-plastic potential function is postulated in which the elastic and plastic contributions are decoupled

$$\Psi = \Psi^e(\mathbf{g}, \mathbf{b}_e^{-1}) + \Psi^p(\mathbf{q}) \tag{4}$$

where $\mathbf{q}$ represents a set of internal variables which describe the path-dependent plastic process.

With eqn (3) plastic dissipation can be written as

$$\mathscr{D}^p = -\mathbf{b}_e^{-1}\, \hat{\partial}_{\mathbf{b}_e^{-1}} \Psi^e : L_v \mathbf{b}_e^{-1} - \partial_{\mathbf{q}} \Psi^p \cdot L_v \mathbf{q} = \frac{1}{\varrho_0} \tau : \mathbf{d}_p + \mathbf{Y} \cdot L_v \mathbf{q} \tag{5}$$

with

$$\mathbf{Y} = -\hat{\partial}_{\mathbf{q}} \Psi^p(\mathbf{q}) \tag{6}$$

and the plastic deformation rate $\mathbf{d}_p = \frac{1}{2} L_v \mathbf{b}_e^{-1}$. In eqn (5) L_v is the Lie-derivative of a time dependent tensor field representing a so-called pull-back operation.

The governing constitutive equations of the rate-independent associative elasto-plastic problem are summarized as follows:

$$
\begin{aligned}
&\Psi = \Psi(\mathbf{g}, \mathbf{b}_e^{-1}, \mathbf{q}) \quad \text{Helmholtz-free energy} \\
&\tau = 2\varrho_0 \frac{\partial \Psi}{\partial \mathbf{g}} = 2\varrho \mathbf{b}_e \frac{\partial \Psi}{\partial \mathbf{b}_e} \quad \text{hyperelastic constitutive relation} \\
&\mathscr{D}^p(\mathbf{g}, \mathbf{b}_e^{-1}, \mathbf{q}; L_v \mathbf{b}_e^{-1}, \mathbf{L}_v \mathbf{q}) \geqslant 0 \quad \text{plastic dissipation} \\
&\phi = \phi(\mathbf{g}, \mathbf{b}_e^{-1}, \mathbf{q}) \leqslant 0 \quad \text{yield surface} \\
&L_v \tau = 2\dot{\lambda} \frac{\partial \phi}{\partial \mathbf{g}}(\mathbf{g}, \mathbf{b}_e^{-1}, \mathbf{q}) \quad \text{associated flow rule} \\
&\dot{\boldsymbol{\alpha}} = \dot{\lambda} \frac{\partial \phi}{\partial \mathbf{q}} \quad \text{evolution equation for internal variables} \\
&\dot{\lambda} \geqslant 0; \phi(\mathbf{g}, \mathbf{b}_e^{-1}, \mathbf{q}) < 0; \dot{\lambda}\phi = 0 \quad \text{loading/unloading (Kuhn–Tucker) conditions.}
\end{aligned}
\tag{7}
$$

The derivation of eqns (7) follows from the application of the principle of maximum plastic dissipation to eqn (5) and is presented in Simo (1988a).

2.1. *J_2-Flow theory*

The constitutive model described above will be applied here to the special case of the J_2-flow theory with isotropic hardening. In this case the set of internal variables $\mathbf{q}$ reduces to a single scalar variable $\bar{\varepsilon}_p$ which represents the equivalent uniaxial plastic strain. In view of the pure deviatoric plastic response the multiplicative split of the deformation gradient into its volumetric and deviatoric parts is advantageous

$$
\mathbf{F} = J^{1/3} \bar{\mathbf{F}} \quad \text{with} \quad \det \bar{\mathbf{F}} = 1. \tag{8}
$$

Based on this decomposition the following decoupled form of the free energy will be introduced [eqn (4)].

$$
W = \tfrac{1}{2}\kappa f(J) + \tfrac{1}{2}\mu g(\bar{\mathbf{F}}_e) + \varrho \psi^p(\bar{\varepsilon}_p) \tag{9}
$$

κ and μ are the bulk and the shear moduli, respectively. According to eqn (3) the Kirchhoff stress is decomposed into the hydrostatic and deviatoric parts

$$
\tau = \mathbf{k} + \mathbf{s}
$$

where

$$
\mathbf{k} = J\kappa \partial_{\mathbf{g}} f(J) = Jp\mathbf{g}^{-1} \quad \text{with} \quad p = \partial_J W = \partial_J f(J) \quad \text{and} \quad \partial_{\mathbf{g}} J = \mathbf{g}^{-1} \tag{10}
$$

and

$$
\mathbf{s} = J\mu \, \partial_{\mathbf{g}} g(\bar{\mathbf{F}}_e).
$$

In this work the free energy function presented in Simo (1988b) will be adopted:

$$
W = \tfrac{1}{2}\kappa (\ln J)^2 + \tfrac{1}{2}\mu (\bar{\mathbf{b}}_e : \mathbf{g} - 3) \tag{11}
$$

where $\bar{\mathbf{b}}_e$ is the modified elastic left Cauchy–Green tensor defined as

$$\mathbf{b}_e := \bar{\mathbf{F}}_e \bar{\mathbf{F}}_e^T = J^{-2/3} \mathbf{F}_e \mathbf{F}_e^T = J^{-2/3} \mathbf{b}_e. \tag{12}$$

Now, according to eqn (7b) the Kirchhoff stress tensor follows

$$\boldsymbol{\tau} = \kappa \ln J \mathbf{g}^{-1} + \mu \operatorname{dev} \bar{\mathbf{b}}_e \quad \text{with} \quad p = \frac{\kappa}{J} \ln J. \tag{13}$$

The special form of eqns (7) for the J_2-flow theory with isotropic hardening and the function for the free energy, defined in eqn (11), is then

$$\begin{aligned}
W &= \varrho \Psi = \{\tfrac{1}{2}\kappa (\ln J)^2 + \tfrac{1}{2}\mu (\mathbf{g} : \bar{\mathbf{b}}_e - 3)\} + \varrho \Psi^p(\bar{\varepsilon}_p) \\
\boldsymbol{\tau} &= \kappa \ln J \mathbf{g}^{-1} + \mu \operatorname{dev} \bar{\mathbf{b}}_e \\
\mathscr{D}^p &= \frac{1}{\varrho} \boldsymbol{\tau} : \mathbf{d}_p + \mathbf{Y} \cdot L_v \bar{\varepsilon}_p \\
\phi &= \phi(\mathbf{g}, \mathbf{s}, \bar{\varepsilon}_p) = \|\mathbf{s}\| - \sqrt{\tfrac{2}{3}} \sigma_y(\bar{\varepsilon}_p) \\
L_v \boldsymbol{\tau} &= \dot{\lambda} \partial_{\mathbf{g}} \phi = 2 \bar{\mu} \dot{\lambda} \frac{\mathbf{s}}{\|\mathbf{s}\|} \\
\dot{\bar{\varepsilon}}_p &= \dot{\lambda} \sqrt{\tfrac{2}{3}}
\end{aligned} \tag{14}$$

where again the principle of maximum plastic dissipation was applied. The hypothesis of small elastic deformations is embedded in eqn (14c), see Simo (1988b). In these equations the deviatoric part of the Kirchhoff stress $\mathbf{s}$ is related to $\bar{\mathbf{b}}_e$ by

$$\mathbf{s} = \operatorname{dev} \boldsymbol{\tau} = \mu (\bar{\mathbf{b}}_e - \tfrac{1}{3} (\bar{\mathbf{b}}_e : \mathbf{g}) \mathbf{g}^{-1}). \tag{15}$$

Furthermore $\bar{\mu}$ is given by

$$\bar{\mu} = \tfrac{1}{3} \mu J^{-2/3} \operatorname{tr} \bar{\mathbf{b}}_e. \tag{16}$$

2.2. *Numerical integration*

The flow rule [eqn (14e)] and the evolution of the internal variables [eqn (14f)] represent a system of coupled differential equations of first order in time and must be integrated for the evaluation of the state variables. The local integration procedure for large strain J_2-plasticity based on Lee's theory consists of an elastic predictor–plastic corrector algorithm which is identical to the classical "radial-return" algorithm for small strain plasticity of Wilkins (1964) as shown in Simo (1988b). This procedure is outlined in its spatial description in Table 1.

3. FINITE ELEMENT FORMULATION

3.1. *Weak formulation of the boundary value problem*

The formulation of the classical weak form of momentum balance in a spatial description restricted to the static case follows

Table 1. Projection method for J_2-flow theory with isotropic hardening

- with the updated geometry

$$\mathbf{x}_{n+1} = \mathbf{x}_n + \mathbf{u}$$

actual deformation gradient (at integration point)

$$\mathbf{F}_{n+1} = \frac{\partial \mathbf{x}_{n+1}}{\partial \mathbf{X}} \tag{17}$$

volumetric/deviatoric split

$$\bar{\mathbf{F}}_{n+1} = J_{n+1}^{-1/3}\mathbf{F}_{n+1}; \quad J_{n+1} := \det[\mathbf{F}_{n+1}] \tag{18}$$

- elastic predictor phase

elastic trial for the modified left Cauchy–Green deformation tensor

$$\bar{\mathbf{b}}_{n+1}^{e^{tr}} = \bar{\mathbf{F}}_{n+1}\mathbf{C}_n^{p-1}\bar{\mathbf{F}}_{n+1}^{T} \tag{19}$$

trial for the stress deviator

$$\mathbf{s}_{n+1}^{tr} = \mu \operatorname{dev}[\bar{\mathbf{b}}_{n+1}^{e^{tr}}] \tag{20}$$

$$\mathbf{n}_{n+1} = \frac{\mathbf{s}_{n+1}^{tr}}{\|\mathbf{s}_{n+1}^{tr}\|}. \tag{21}$$

- check for yielding

$$\phi_{n+1}^{tr} = \|\mathbf{s}_{n+1}^{tr}\| - \sqrt{\tfrac{2}{3}}\sigma_y(\bar{\varepsilon}^p) \tag{22}$$

if $\phi_{n+1}^{tr} \leqslant 0 \Rightarrow$ elastic step $\Rightarrow$ set$(\cdot)_{n+1} = (\cdot)_{n+1}^{tr}$ (exact solution) EXIT

if $\phi_{n+1}^{tr} > 0 \Rightarrow$ plastic step $\Rightarrow$ proceed with corrector phase.

- plastic corrector phase

solution for $\Delta\lambda$

$$\|\mathbf{s}_{n+1}^{tr}\| - \Delta S^p(\Delta\lambda) - \sqrt{\tfrac{2}{3}}\sigma_y(\bar{\varepsilon}^p(\Delta\lambda)) = 0 \tag{23}$$

with

$$\Delta S^p = 2\bar{\mu}_{n+1}\Delta\lambda \quad \text{and} \quad \bar{\mu}_{n+1} = \tfrac{1}{3}\mu \operatorname{tr}\bar{\mathbf{b}}_{n+1}^{e^{tr}} \tag{24}$$

return mapping

$$\mathbf{s}_{n+1} = \mathbf{s}_{n+1}^{tr} - 2\bar{\mu}\Delta\lambda\mathbf{n}_{n+1} \tag{25}$$

$$\bar{\varepsilon}_{n+1}^{p} = \bar{\varepsilon}_n^{p} + \sqrt{\tfrac{2}{3}}\Delta\lambda \tag{26}$$

- update the intermediate configuration

$$\bar{\mathbf{b}}_{n+1}^{e} = \bar{\mathbf{b}}_{n+1}^{e^{tr}} - \frac{2\bar{\mu}\Delta\lambda}{\mu}\mathbf{n}_{n+1}. \tag{27}$$

$$g = \int_B \boldsymbol{\sigma} : \operatorname{grad}\delta\mathbf{u}\,dv - \int_B \varrho\mathbf{b}\cdot\delta\mathbf{u}\,dv - \int_{\partial B_\sigma} \bar{\mathbf{t}}\cdot\delta\mathbf{u}\,da \tag{28}$$

with Cauchy stresses $\boldsymbol{\sigma}$, body forces $\mathbf{b}$ and prescribed surface tractions $\bar{\mathbf{t}}$.

For cases where the stresses are computed from a potential function and the loads are conservative it is possible to construct a functional from eqn (28).

$$\Pi(\Phi) = \int_B \hat{W}(\mathbf{X}, \mathbf{F}^T\mathbf{F})\,dv + \Pi^a(\mathbf{X}, \mathbf{u}) \tag{29}$$

where $\hat{W}$ is a potential function of the deformation energy which satisfies the condition of spatial covariance.

Since our main goal in this section is the development of a mixed type finite element formulation, the more general three-field Hu–Washizu variational principle is selected as the basis for the enhanced assumed strain (EAS) formulation proposed by Simo and Rifai

(1990). In this concept the strain fields are enriched through extra functions chosen in such a way that the locking effects diminish and convergence properties are improved. In Simo and Rifai (1990) the EAS concept is applied to the geometrically linear theory. Extensions of the method for three-dimensional plasticity computations are presented in Andelfinger (1992), Simo and Armero (1992), and Roehl (1994) for the complete nonlinear regime. For the large strain version of these elements the three-field functional is derived from eqn (29) introducing an additional field variable $\mathbf{Z}$ with the constraint

$$\mathrm{Grad}\mathbf{u}-\mathbf{Z}=0 \tag{30}$$

so that the Lagrange functional follows as a special case of the Hu–Washizu principle, now referred to the reference configuration

$$\Pi(\mathbf{u},\mathbf{Z},\mathbf{P})=\int_{B_0}\hat{W}(\mathbf{X},[1+\mathbf{Z}]^{\mathrm{T}}[1+\mathbf{Z}])+\mathbf{P}\cdot(\mathrm{Grad}\,\mathbf{u}-\mathbf{Z})\,\mathrm{d}V+\Pi^{\mathrm{a}}(\mathbf{X},\mathbf{u}). \tag{31}$$

The first Piola–Kirchhoff stress tensor $\mathbf{P}$ plays the role of the Lagrange multiplier. The compatible displacement gradient Grad$\mathbf{u}$ is enhanced by additional functions $\tilde{\mathbf{H}}$ so that the total displacement gradient reads

$$\tilde{\mathbf{Z}}=\mathrm{Grad}\,\mathbf{u}+\tilde{\mathbf{H}}. \tag{32}$$

According to eqn (32) the deformation gradient is modified to

$$\tilde{\mathbf{F}}:=1+\tilde{\mathbf{Z}}=1+\mathrm{Grad}\,\mathbf{u}+\tilde{\mathbf{H}}=\mathbf{F}_{\Phi}+\tilde{\mathbf{H}} \tag{33}$$

and the functional (31) can be written as

$$\tilde{\Pi}(\mathbf{u},\tilde{\mathbf{H}},\mathbf{P})=\int_{B_0}\{\hat{W}(\mathbf{X},\tilde{\mathbf{F}}^{\mathrm{T}}\tilde{\mathbf{F}})-\mathbf{P}\cdot\tilde{\mathbf{H}}\}\,\mathrm{d}V+\Pi^{\mathrm{a}}(\mathbf{X},\mathbf{u}). \tag{34}$$

The first variation of eqn (34) at $(\mathbf{u},\tilde{\mathbf{H}},\mathbf{P})$ in direction $(\delta\mathbf{u},\delta\tilde{\mathbf{H}},\delta\mathbf{P})$ follows

$$\delta\tilde{\Pi}:=\int_{B_0}[\mathrm{Grad}\,(\delta\mathbf{u})\cdot(2\tilde{\mathbf{F}}\,\partial_{\mathrm{C}}\hat{W})]-\delta\mathbf{P}\cdot\tilde{\mathbf{H}}+\delta\tilde{\mathbf{H}}\cdot[-\mathbf{P}+(2\tilde{\mathbf{F}}\,\partial_{\mathrm{C}}\hat{W})]\,\mathrm{d}V-\delta\Pi^{\mathrm{a}}\cdot(\delta\mathbf{u}). \tag{35}$$

The equivalent spatial version of eqn (35) is obtained through the usual tensor transformations performed with the modified deformation gradient eqn (33)

$$\delta\tilde{\Pi}:=\int_{B_0}\tilde{\nabla}(\delta\mathbf{u})\cdot\tilde{\boldsymbol{\tau}}(\mathbf{u},\tilde{\mathbf{h}})-\delta\boldsymbol{\tau}\cdot\tilde{\mathbf{h}}+\delta\tilde{\mathbf{h}}\cdot[-\boldsymbol{\tau}+\tilde{\boldsymbol{\tau}}(\mathbf{u},\tilde{\mathbf{h}})]\,\mathrm{d}V+\delta\Pi^{\mathrm{a}}(\delta\mathbf{u})=0 \tag{36}$$

where the following definition is introduced

$$\tilde{\mathrm{grad}}\,\delta\mathbf{u}=\tilde{\nabla}(\delta\mathbf{u}):=\mathrm{Grad}\,(\delta\mathbf{u})\tilde{\mathbf{F}}^{-1} \tag{37}$$

$\boldsymbol{\tau}$ is again the Kirchhoff stress tensor; $\tilde{\mathbf{h}}$ is the spatial equivalent to $\tilde{\mathbf{H}}$, i.e. $\tilde{\mathbf{h}}:=\tilde{\nabla}\tilde{\mathbf{F}}^{-1}$.

3.2. *Finite element discretization*

Following the standard methodology a region B is discretized into subregions B_{e} in such a way that

$$B = \bigcup_{i=1}^{n_e} B_e^i; \quad B_e^i \cup B_e^i = \varnothing.$$

We consider here general three-dimensional isoparametric elements so that over a typical element B_e the geometry and local displacement fields are expressed in the form

$$\mathbf{X}^h = \sum_{k=1}^{NN} \mathbf{N}^k(\xi)\mathbf{X}_k^e; \quad \mathbf{x}^h = \sum_{k=1}^{NN} \mathbf{N}^k(\xi)\mathbf{x}_k^e; \quad \mathbf{u}^h = \sum_{k=1}^{NN} \mathbf{N}^k(\xi)\mathbf{d}_k^e \tag{38}$$

where NN indicates the number of element nodes, $\mathbf{X}_k$, $\mathbf{x}_k$, $\mathbf{d}_k \in \mathscr{R}^3$ $(k = 1, 2, \ldots NN)$ are, respectively, the node vectors in the reference and current configurations, and the node displacements. $\mathbf{N}^k: \square \to \mathscr{R}$ are the corresponding shape functions defined in the natural coordinates ξ of the unit cube $\square: [-1,1] \times [-1,1] \times [-1,1]$. With the above approximations the expression for the discrete compatible deformation gradient in matrix format follows

$$\mathbf{F}_\Phi^h(\xi, t) = \sum_{k=1}^{NN} \mathbf{x}_k^e(t) \cdot \mathrm{Grad}\,[N^k]$$

with

$$\mathbf{x}_k^e(t) = [x_k^1, x_k^2, x_k^3]_e^{\mathrm{T}} = \mathbf{X}_k^e + \mathbf{d}_k^e(t)$$

and

$$\mathrm{Grad}\,[N^k] = [N_{,1}^k, N_{,2}^k, N_{,3}^k]. \tag{39}$$

$\mathrm{Grad}\,(\cdot)$ denotes the gradient with respect to the coordinates $\mathbf{X}$. The matrix $\mathrm{Grad}[N^k]$ is obtained applying the chain rule

$$\mathrm{Grad}\,[N^k] = \mathbf{J}(\xi)^{-\mathrm{T}} \mathrm{Grad}_\xi\,[N^k] \tag{40}$$

where $\mathbf{J}(\xi)$ is the Jacobian matrix

$$\mathbf{J}(\xi) = \frac{\partial \mathbf{X}_e^h(\xi)}{\partial \xi}. \tag{41}$$

3.3. *EAS formulation for large deformations*

For the mixed finite element formulation in addition to the standard approximations for the displacements (38) trials for the new field variables $\tilde{\mathbf{H}}$ are necessary. In view of a spatial formulation of the boundary value problem (36) the interpolations of the enhanced displacement gradient $\tilde{\mathbf{H}}$ will be defined in the reference configuration and subsequently transformed into its spatial counterpart $\tilde{\mathbf{h}}$. Corresponding to eqn (33) the discrete form of the enriched deformation gradient $\tilde{\mathbf{F}}$ is

$$\tilde{\mathbf{F}}^h = \mathbf{F}_\Phi^h + \tilde{\mathbf{H}}^h. \tag{42}$$

- Additive form does not satisfy incremental patch test.
- Multiplicative decomposition of $\tilde{\mathbf{F}}^h$ is better, as in ABAQUS (Theory Manual) incompatible modes elements,

where $\tilde{\mathbf{F}}_\Phi^h$ is defined in eqn (39). The field $\tilde{\mathbf{H}}$ is an extra field which, according to the underlying variational principle, does not have to satisfy continuity requirements at the element boundaries. Analogous to the compatible displacement gradient, the enhanced deformation gradient can be written as

$$\tilde{\mathbf{H}}_e^h(\xi, t) = \sum_{I=1}^{N\alpha} \boldsymbol{\alpha}_I^e(t) \cdot \mathbf{G}_e^I$$

where

$$\boldsymbol{\alpha}_I = [\alpha_I^1, \alpha_I^2, \alpha_I^3]^T \quad \text{and} \quad \mathbf{G}^I = [G_1^I, G_2^I, G_3^I]. \tag{43}$$

The vectors α_I $(I = 1, 2, \ldots, N\alpha)$ contain each, three local parameters and $\mathbf{G}_e^I : \square \mapsto B_0$ are vectors of the additional interpolation functions.

As observed in Simo and Rifai (1990) the functions $\mathbf{G}^I$ can be understood in conjunction with eqn (39) as the derivatives of form functions of an incompatible displacement field $\tilde{\mathbf{u}}^h$ with respect to the reference coordinates $\mathbf{X}$.

$$\tilde{\mathbf{u}}^h = \sum_{I=1}^{N\alpha} \tilde{N}^I(\xi) \boldsymbol{\alpha}_I^e$$

and

$$\operatorname{Grad} \tilde{\mathbf{u}}_e^h(\xi, t) = \sum_{I=1}^{N\alpha} \boldsymbol{\alpha}_1^e(t) \cdot \mathbf{G}_e^I = \sum_{I=1}^{N\alpha} \boldsymbol{\alpha}_1^e(t) \cdot \operatorname{Grad}[\tilde{N}^I]$$

with

$$\operatorname{Grad}[\tilde{N}^I] = [\tilde{N}^I{}_{,1}, \tilde{N}^I{}_{,2}, \tilde{N}^I{}_{,3}]. \tag{44}$$

This analogy is only ideal since it is not always possible to explicitly furnish a set of functions $\tilde{N}^I$ for every set of functions $\mathbf{G}^I$.

The choice of the functions $\tilde{\mathbf{H}}^h$ is subject to some conditions which guarantee stability and convergence of the method (Reddy and Simo, 1992; Simo and Rifai, 1990). The first condition requires that the space E^h of the compatible functions $\mathbf{F}_\Phi^h$ and the space $\tilde{E}^h$ of the enhanced functions $\tilde{\mathbf{H}}^h$ be independent from each other:

• Condition 1:

$$E^h \cap \tilde{E}^h = \varnothing. \tag{45}$$

This condition guarantees stability of the method for the linearized problem and excludes functions which lead to a rank deficient element.

The second condition requires that the space $\tilde{E}^h$ of the enhanced functions be L_2-orthogonal to the space T^h of the admissible stresses. This condition can be expressed as

• Condition 2:

$$\langle \mathbf{P}^h, \delta\tilde{\mathbf{H}}^h \rangle_{L_2(B)} := \int_{B_0} \mathbf{P}^h \cdot \delta\tilde{\mathbf{H}}^h \, \mathrm{d}V = 0$$

or equivalently,

$$\langle \boldsymbol{\tau}^h, \delta\tilde{\mathbf{h}}^h \rangle_{L_2(B)} := \int_{B_0} \boldsymbol{\tau}^h \cdot \delta\tilde{\mathbf{h}}^h \, \mathrm{d}V = 0 \quad \forall \, \delta\tilde{\mathbf{H}}^h, \delta\tilde{\mathbf{h}}^h \in \tilde{E}^h. \tag{46}$$

Equation (46) requires that at least element-wise constant stresses $\boldsymbol{\tau}_0$ are present in T^h, for which the orthogonality condition reads

$$\langle \boldsymbol{\tau}_0, \delta\tilde{\mathbf{h}}^h \rangle = 0. \tag{47}$$

Furthermore, the approximations $\tilde{\mathbf{H}}^h$ have to be material covariant, so that the deformation

gradient defined in eqn (42) satisfies the objectivity requirement of the constitutive equations. The introduction of the orthogonality condition (46) in the variational equation (36) leads to an equation which is independent from the stress field $\boldsymbol{\tau}^h$

$$\delta\tilde{\Pi} := \int_{B_0} \tilde{\nabla}(\delta\mathbf{u}^h) \cdot \tilde{\boldsymbol{\tau}}(\mathbf{u}^h, \tilde{\mathbf{h}}^h) + \delta\tilde{\mathbf{h}}^h \cdot \tilde{\boldsymbol{\tau}}(\mathbf{u}^h, \tilde{\mathbf{h}}^h)\, \mathrm{d}V + \Pi^a(\delta\mathbf{u}^h) = 0 \tag{48}$$

where the operator $\tilde{\nabla}(\cdot)$ is defined in eqn (37) and $\tilde{\boldsymbol{\tau}}(\mathbf{u}^h, \tilde{\mathbf{h}}^h)$ follows from the discrete form of the constitutive relation

$$\tilde{\boldsymbol{\tau}}(\mathbf{u}^h, \tilde{\mathbf{h}}^h) := [2\tilde{\mathbf{F}}^h\, \partial_{\mathbf{C}} \hat{W}(\mathbf{X}, \tilde{\mathbf{F}}^{h^{\mathrm{T}}}\mathbf{F}^h)]. \tag{49}$$

The linearization of eqn (48) renders the discrete tangent which in matrix notation reads

$$\begin{aligned}
&[\delta\mathbf{d}^h]^{\mathrm{T}} \left\{ \int_{B_{0_e}} \mathbf{B}^{\mathrm{T}} J\mathbb{C}\mathbf{B}\, \mathrm{d}V + \int_{B_{0_e}} \mathbf{B}_{\mathrm{G}}^{\mathrm{T}} \tilde{\boldsymbol{\tau}} \mathbf{B}_{\mathrm{G}}\, \mathrm{d}V \right\} [\mathbf{d}^h] + [\delta\mathbf{d}^h]^{\mathrm{T}} \left\{ \int_{B_{0_e}} \mathbf{B}^{\mathrm{T}} J\mathbb{C}\tilde{\mathbf{B}}\, \mathrm{d}V + \int_{B_{0_e}} \mathbf{B}_{\mathrm{G}}^{\mathrm{T}} \tilde{\boldsymbol{\tau}} \tilde{\mathbf{B}}_{\mathrm{G}}\, \mathrm{d}V \right\} [\boldsymbol{\alpha}^h] \\
&+ [\delta\boldsymbol{\alpha}^h]^{\mathrm{T}} \left\{ \int_{B_{0_e}} \tilde{\mathbf{B}}^{\mathrm{T}} J\mathbb{C}\mathbf{B}\, \mathrm{d}V + \int_{B_{0_e}} \tilde{\mathbf{B}}_{\mathrm{G}}^{\mathrm{T}} \tilde{\boldsymbol{\tau}} \tilde{\mathbf{B}}_{\mathrm{G}}\, \mathrm{d}V \right\} [\boldsymbol{\alpha}^h] + [\delta\boldsymbol{\alpha}^h]^{\mathrm{T}} \left\{ \int_{B_{0_e}} \tilde{\mathbf{B}}^{\mathrm{T}} J\mathbb{C}\mathbf{B}\, \mathrm{d}V + \int_{B_{0_e}} \tilde{\mathbf{B}}_{\mathrm{G}}^{\mathrm{T}} \tilde{\boldsymbol{\tau}} \mathbf{B}_{\mathrm{G}}\, \mathrm{d}V \right\} [\mathbf{d}^h].
\end{aligned} \tag{50}$$

Following the usual procedure of the finite element method the matrices $\mathbf{B}$ and $\mathbf{B}_{\mathrm{G}}$ contain the derivatives of N^{K} with respect to the spatial coordinates $\mathbf{x}_J$ ($J = 1, 2, 3$) ordered in such a way that the components of the vector of the displacement gradients can be determined as

$$\tilde{\nabla}^s \mathbf{u}^h =: \mathbf{B}^h \mathbf{d}^h; \quad \delta(\tilde{\nabla}^s \mathbf{u}^h) =: \mathbf{B}^h \delta\mathbf{d}^h. \tag{51}$$

Similarly its enhanced part leads to matrices $\tilde{\mathbf{B}}$ and $\tilde{\mathbf{B}}_{\mathrm{G}}$:

$$\tilde{\nabla}^s \tilde{\mathbf{u}}^h =: \tilde{\mathbf{B}}^h \boldsymbol{\alpha}^h; \quad \delta(\tilde{\nabla}^s \tilde{\mathbf{u}}^h) =: \tilde{\mathbf{B}}^h \boldsymbol{\alpha}^h. \tag{52}$$

The implementation of the EAS concept in a nonlinear solution strategy follows in the usual way and is summarized in Appendix A. Once the local parameters α are eliminated on the element level the number of global unknowns is the same as for the displacement model. In addition, the EAS concept is advantageous for applications of plasticity since the return algorithms, for example the radial return concept of Table 1, do not need a modification for the mixed model.

3.4. *Application of the EAS concept to brick elements*

In view of conditions 1 and 2, eqns (45) and (46), the enhanced field $\tilde{\mathbf{H}}$ is interpolated in parametric coordinates and subsequently transformed into the real space. Point of departure are functions $\mathbf{M}_\xi : \square \mapsto \square$ defined in the local element coordinate system which satisfy

$$\int_{\square} \mathbf{M}(\xi)\, \mathrm{d}\square = 0. \tag{53}$$

According to condition 1 the functions in $\mathbf{M}_\xi(3 \times n\alpha/3)$ are not present in the interpolations $\mathrm{Grad}_\xi[\mathbf{u}^h]$. These functions are transformed to the reference configuration

$$\mathbf{G}_e(\xi) = \frac{j_0}{j(\xi)} \mathbf{J}_0^{-T} \mathbf{M}(\xi) \tag{54}$$

where $\mathbf{J}_0$ is the Jacobian matrix of the isoparametric map evaluated at the centroid of the element, j_0 is its determinant, i.e. $j_0 = \det \mathbf{J}_0$, and j corresponds to the determinant of the Jacobian matrix at an integration point ξ. The use of $\mathbf{J}_0$ instead of $\mathbf{J}$ was suggested by Taylor *et al.* (1986) for the satisfaction of the patch test in the case of incompatible elements. The mapping $\tilde{\mathbf{H}}^h(\xi): B_0 \mapsto \Phi^h(B_0)$ follows then from eqns (43) and (54)

$$\tilde{\mathbf{H}}^h = \sum_{I=1}^{n\alpha} \boldsymbol{\alpha}_I^e \cdot \mathbf{G}_e^I = \sum_{I=1}^{n\alpha} \boldsymbol{\alpha}_I^e \cdot \left[\frac{j_0}{j(\xi)} \mathbf{J}_0^{-1} \mathbf{M}(\xi) \right]^I. \tag{55}$$

Here the EAS concept will be applied to the trilinear hexahedral element HEXA8 which is well known for its excessively stiff behaviour in bending and nearly incompressible conditions. Improvements of this element using this concept are presented by Simo and Rifai (1990) and Andelfinger *et al.* (1992) for small deformations and for the fully nonlinear analysis by Simo and Armero (1992), and Roehl (1994). The polynomial terms included in $\mathbf{M}_\xi$ are chosen by inspection of the interpolations of the deformation gradient so that the spaces E^h and $\tilde{E}^h$ are independent.

The shape functions associated with the HEXA8 element are given in the following. The usual terms present in the displacement gradients and the missing ones of a trilinear interpolation are shown for completeness.

$$\Phi^h: 1 \quad \xi \quad \eta \quad \zeta \quad \xi\eta \quad \xi\zeta \quad \eta\zeta \quad \xi\eta\zeta \tag{56}$$

existing terms | missing terms

$$\begin{array}{lcccccccc|ccccccccc}
\Phi^h_{,\xi}: & 0 & 1 & 0 & 0 & \eta & \zeta & 0 & \eta\zeta & \xi & 0 & 0 & \xi\eta & 0 & 0 & \xi\zeta & 0 & 0 \\
\Phi^h_{,\eta}: & 0 & 0 & 1 & 0 & \xi & 0 & \zeta & \xi\zeta & 0 & \eta & 0 & 0 & \eta\zeta & 0 & 0 & \eta\xi & 0 \\
\Phi^h_{,\zeta}: & 0 & 0 & 0 & 1 & 0 & \xi & \eta & \xi\eta & 0 & 0 & \zeta & 0 & 0 & \zeta\xi & 0 & 0 & \zeta\eta
\end{array}.$$

Adopting for $\mathbf{M}_\xi$ an interpolation with the first three terms ($n\alpha = 3$) the modified deformation gradient includes complete linear polynomials

$$\mathbf{M}_\xi = \begin{bmatrix} \xi & 0 & 0 \\ 0 & \eta & 0 \\ 0 & 0 & \zeta \end{bmatrix}. \tag{57}$$

For distorted elements and in the incompressible limit this enhancement does not completely eliminate locking (Andelfinger *et al.*, 1992; Andelfinger and Ramm, 1993). Therefore, an extension of $\mathbf{M}_\xi$ with the following three terms ($n\alpha = 6$) is suggested here

$$\mathbf{M}_\xi = \begin{bmatrix} \xi & 0 & 0 & \xi\eta & 0 & 0 \\ 0 & \eta & 0 & 0 & \eta\zeta & 0 \\ 0 & 0 & \zeta & 0 & 0 & \zeta\xi \end{bmatrix}. \tag{58}$$

The enhanced elements are denoted by HEXA8-E3 and HEXA8-E6, respectively. It can be shown that the element based on $\mathbf{M}_\xi$ given in eqn (57) may yield hourglass modes at high compressive strains when they are under-integrated by the conventional eight-point Gaussian quadrature. It was pointed out by Simo *et al.* (1993) that a different integration rule with nine points may overcome this problem; but different from Simo *et al.* (1993) in

Table 2. Integration rules

Rule	A_1	B_6	C_8	b	c
9	3.555556	0.000000	0.555556	0.000000	0.745356
15a	1.564444	0.355556	0.537778	1.000000	0.674100
15b	0.712137	0.686227	0.396312	0.848418	0.727662

Table 3. Eigenvalues of non-distorted element for incompressible material

	HEXA8	HEXA8-E3	HEXA8-E6
1	0.0555	0.0555	0.0555
2	0.0555	0.0555	0.0555
3	0.1666	0.1111	0.0926
4	0.1666	0.1111	0.0926
5	0.1666	0.1111	0.0926
6	0.2222	0.2222	0.1111
7	0.3333	0.3333	0.1111
8	0.3333	0.3333	0.1111
9	0.3333	0.3333	0.2222
10	0.3333	0.3333	0.3333
11	0.3333	0.3333	0.3333
12	∞	0.3333	0.3333
13	∞	0.3333	0.3333
14	∞	0.3333	0.3333
15	∞	∞	0.3333
16	∞	∞	0.3333
17	∞	∞	0.3333
18	∞	∞	∞

the present study a 15-point integration rule (Irons, 1971) in two versions has been used which gives excellent results (Table 2).

$$\int_{\square} f(\xi)\,\mathrm{d}\square = A_1 f(0,0,0) + B_6[f(-b,0,0)+f(b,0,0)+f(0,-b,0)+\ldots(6\text{ terms})] + C_8[f(-c,-c,-c)+f(c,-c,-c)+\ldots(8\text{ terms})] \tag{59}$$

3.5. *Element tests*

3.5.1. *Eigenvalue analysis.* The EAS extensions HEXA8-E3 and HEXA8-E6 to the conventional displacement model HEXA8 have been investigated by an eigenvalue analysis for the unit cube. Poisson's ratio is taken as 0.49999, simulating the almost incompressible limit. This allows for only one eigenvalue which tends to infinity, thus representing a pure dilatational mode. In Table 3 the 18 non-zero eigenvalues are listed. It can be seen that only the HEXA8-E6 is able to verify the mentioned requirement, whereas both other elements still tend to lock in the incompressible limit.

It should be noted that the EAS elements also satisfy the patch test for arbitrarily distorted geometries.

3.5.2. *Element distortion.* The sensitivity with respect to element distortion has been investigated by a cantilever beam with two elements defined by the distortion parameter e, Fig. 3. The beam has a length of 10 and a cross-section of 2×2. The material parameters are $E = 1500$ and $\nu = 0.25$.

Figure 4 shows the vertical displacement W_A of point A normalized to the exact solution versus the distortion parameter e. As with other hybrid elements both EAS elements are still distortion sensitive, however, a considerable improvement over the pure displacement model can be obtained.

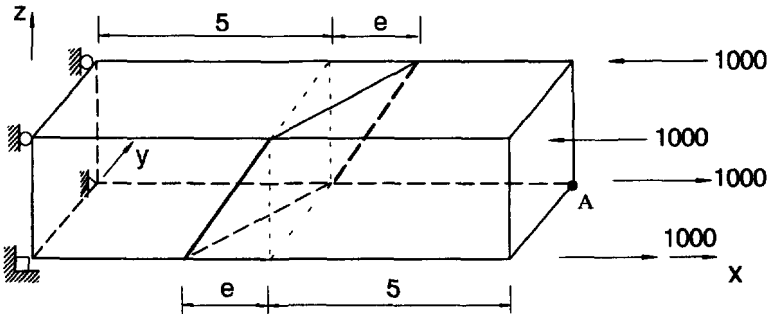

Fig. 3. Cantilever with distorted mesh.

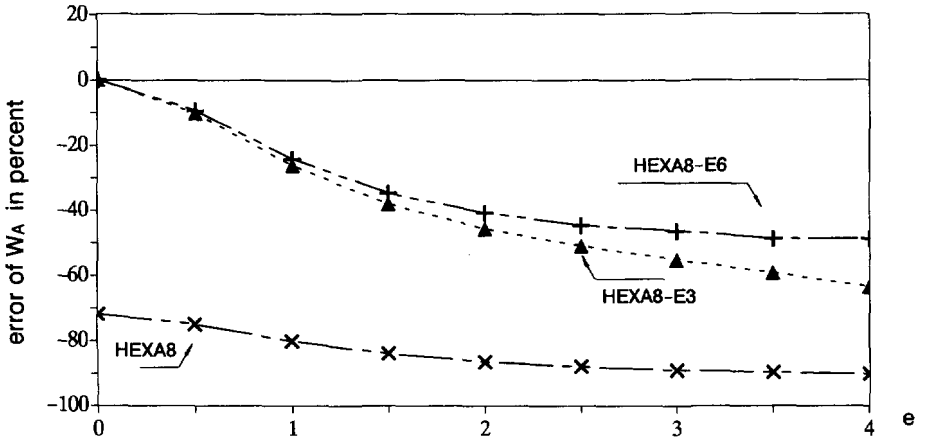

Fig. 4. Vertical displacements W_A.

3.5.3. *Thickness locking.* A simply supported square plate under uniform load ($E = 10^7$ N/cm^2, $\nu = 0.3$, $L = 100$ cm) has been analyzed for three different length to thickness ratios $L/h = 10^2/10^3/10^4$. Uniform meshes with $2 \times 2/3 \times 3/4 \times 4$ elements per quarter of the plate have been used. In Table 4 the results for the centre displacement normalized to the exact solution of a Kirchhoff plate are listed. It can be recognized that the HEXA8-E3 element still shows considerable shear locking, whereas the six parameter model renders sufficient results even for an extremely thin plate.

4. NUMERICAL EXAMPLES FOR LARGE ELASTO-PLASTIC DEFORMATIONS

In the following examples the above described material model with a logarithmic free energy, von Mises yield criterion and an associative flow rule has been adopted.

4.1. *Thick-walled cylinder under internal pressure*

Due to the symmetry of the infinitely long cylinder only one sector with plane strain conditions as indicated in Fig. 5 needs to be analyzed. Ideal plasticity with the given material parameters is assumed which almost approximates a rigid plastic response. The structure is loaded by 15 increments controlling the internal radial displacement from 10 mm at the

Table 4. Normalized displacement of simply supported plate

	$L/h = 10^2$			$L/h = 10^3$			$L/h = 10^4$		
	2×2	3×3	4×4	2×2	3×3	4×4	2×2	3×3	4×4
HEXA8	0.009	0.020	0.035	0.000	0.000	0.000	0.000	0.000	0.000
HEXA8-E3	0.142	0.466	0.737	0.002	0.009	0.027	0.000	0.000	0.000
HEXA8-E6	0.990	0.997	0.999	0.990	0.996	0.998	1.000	1.015	1.098

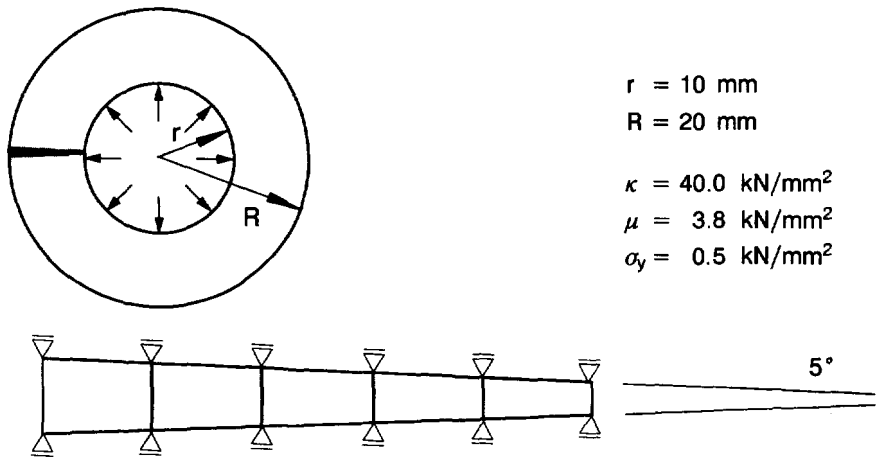

Fig. 5. Thick-walled cylinder.

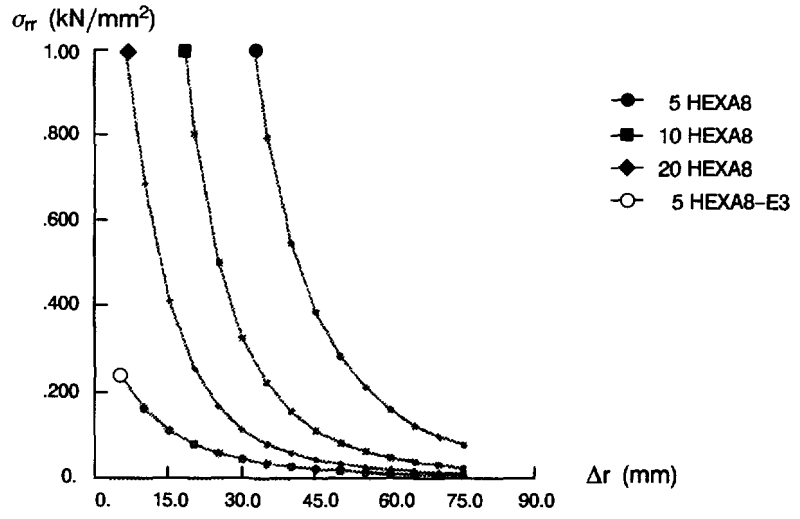

Fig. 6. Evolution of radial stresses σ_{rr} during deformation.

beginning to the final value of 85 mm. The thickness decreases from 10 mm to 1.75 mm during loading.

In Fig. 6 the evolution of the radial stresses σ_{rr} during loading is plotted vs the change of the internal radius Δr. It can be seen that the pure displacement model HEXA8 with 5, 10, 20 elements is incapable of verifying the incompressible state. In contrast to this the EAS extension with three extra modes already coincides with the exact solution (not specifically indicated) when only five elements are used.

It should be noted that the conventional $2 \times 2 \times 2$ Gauss integration did lead to element pathologies with zero-energy modes already in the low loading range. These problems could be overcome resorting to the nine or 15a integration rule described in Section 3.4.

4.2. *Compressed hollow cylinder*

A thick ($H/d = 3.8$) and a thinner ($H/d = 1.7$) hollow cylinder, as defined in Fig. 7, are compressed by a displacement controlled loading with a non-slip condition at the lower and upper boundaries. Again, ideal plasticity without hardening is assumed.

A 5° segment of one half of the cylinder has been idealized by a 12×12 finite element mesh. The experimental response of the two cylinders has been discussed by Nadai (1950) who pointed out the completely different deformation patterns of both structures. The evolution of the shear bands c is indicated in Fig. 8 for the two cylinders.

The result of the numerical simulation for the deformations is given in Fig. 9. It can be clearly seen that the pure displacement model HEXA8 is in both cases not able to verify

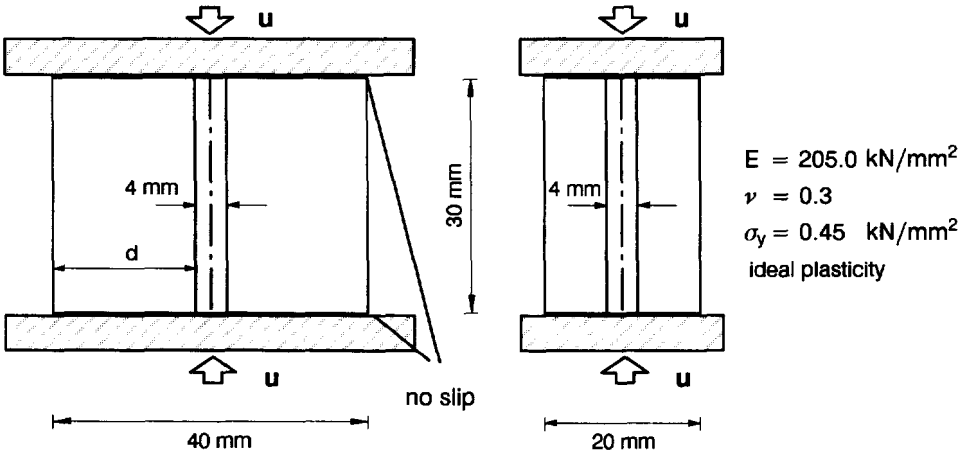

Fig. 7. Compressed hollow cylinder.

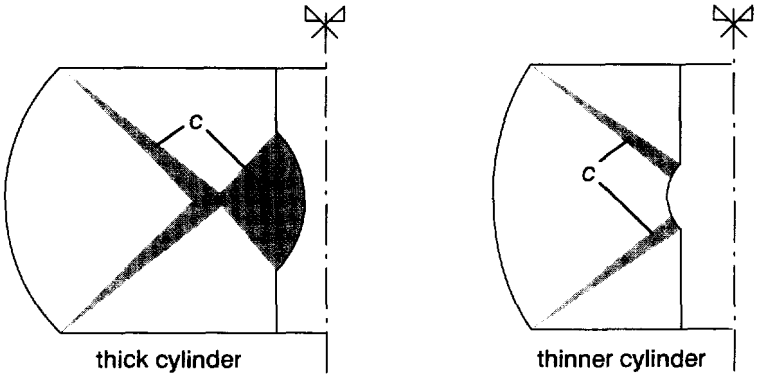

Fig. 8. Deformation pattern of compressed cylinders (Nadai, 1950).

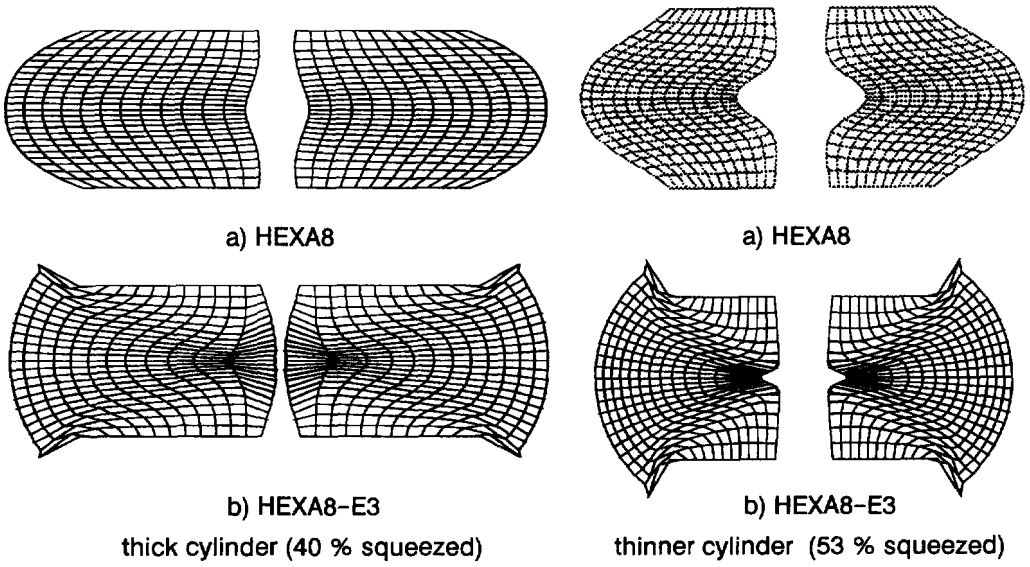

Fig. 9. Deformed compressed cylinders.

the related pattern, whereas the EAS element with only three extra modes shows the correct mode as well as the corresponding shear bands. This is also reflected in the load–deflection diagrams (Fig. 10).

Both cylinders are also analyzed by the conventional ("additive") small strain plasticity (Fig. 11). The different response comes along with a totally different evolution of the plastic

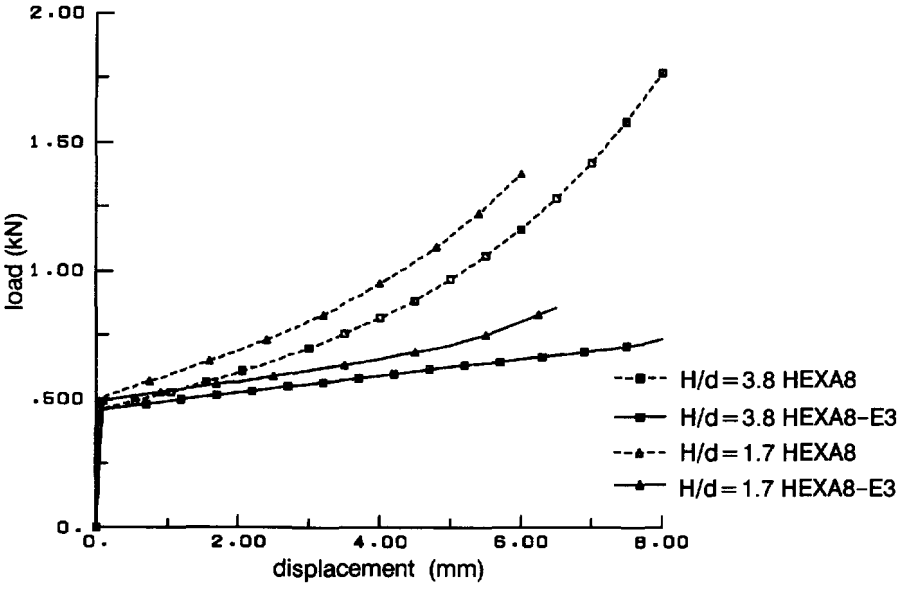

Fig. 10. Load–deflection diagram of hollow cylinder.

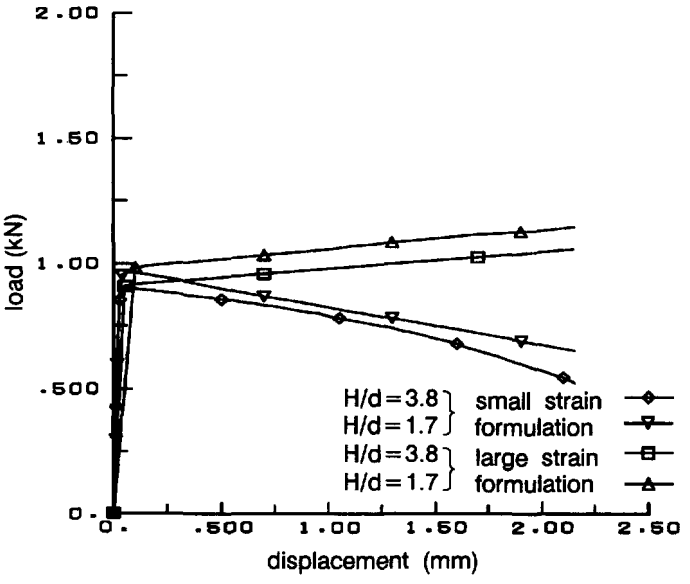

Fig. 11. Small vs large strain formulation.

strains. In contrast to the ("multiplicative") large strain formulation the plastic strains are much more concentrated in the centre part of the cylinder and spread more in a radial than diagonal direction.

Further examples are given in Büchter *et al.* (1994).

5. APPLICATION OF THREE-DIMENSIONAL MATERIAL LAWS TO THIN-WALLED STRUCTURES

5.1. *Motivation*

The traditional approach for thin-walled structures like plates and shells is to reduce the constitutive law to the set of stresses and strains relevant in the corresponding theory; usually all transverse stresses are eliminated in a Kirchhoff–Love theory or the normal stresses–strains in thickness direction are not taken into account whenever Reissner–Mindlin kinematics are used. For a complex material law like the one used in the present study the reduction is not explicitly possible and needs extra considerations. If large strains

become dominant the reduction is even mechanically not feasible. Therefore, it might be desirable to resort to a complete three-dimensional constitutive law. It is well known that the simple application of brick elements with a linear displacement field across the thickness which actually satisfies the typical plate/shell assumption does lead to a considerable error. The too stiff behaviour which could be termed "thickness locking" is due to an imbalance between the transverse normal stress and strain interpolation across the thickness. For a linear elastic material it turns out that the strains E_{33} are constant although the stresses S^{33} are linear through the thickness. This problem has been extensively discussed by Büchter and Ramm (1992), where also a remedy was proposed in the context of a three-dimensional shell formulation, augmenting the theory by a linear strain term E_{33}. This extra variable is also added in the EAS sense following a hybrid approach, i.e. the extra unknown can be eliminated at the element level returning to a conventional displacement formulation. For details of the formulation see Büchter *et al.* (1994).

This extension allows the application of the described three-dimensional large strain elasto-plastic material model directly to the plate/shell formulation. It should be noted that in this case the modified metric

$$\mathbf{g}^* = \mathbf{G} + 2(\mathbf{E} + \bar{\mathbf{E}}) \tag{60}$$

has to be supplied for the deformation gradient and the material tangent.

In the following examples the classical eight-node shell element with reduced integration is employed. The extra parameter for the linear strain term is interpolated in a bilinear way across the element. The results of this so-called seven-parameter theory are compared to a conventional five-parameter model with Reissner/Mindlin kinematics, a simple extension to a six-parameter formulation including the thickness change and to the continuum solution with EAS extension described above. The five-parameter model is restricted to small strain plasticity which seems to be a reasonable approximation for these small strain problems.

5.2. *Pinched hemispherical shell*

Figure 12 shows one quarter of the hemispherical shell with a free edge pinched by two couples of concentrated loads. The geometrical and material data are given. The deformed shell is shown in Fig. 13.

One hundred and ninety two finite shell elements are used. The results of the six- and seven-parameter formulation are compared to a corresponding analysis with HEXA8-E3 elements. The load deflection diagram for the two points A and B is given in Fig. 14. It can be noticed that the seven-parameter formulation comes very close to the three-dimensional

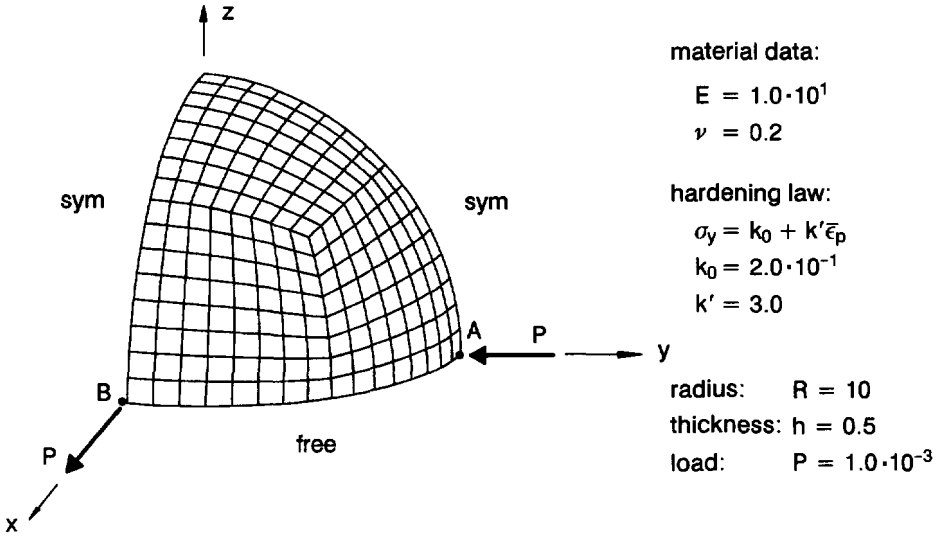

Fig. 12. Hemispherical shell: data.

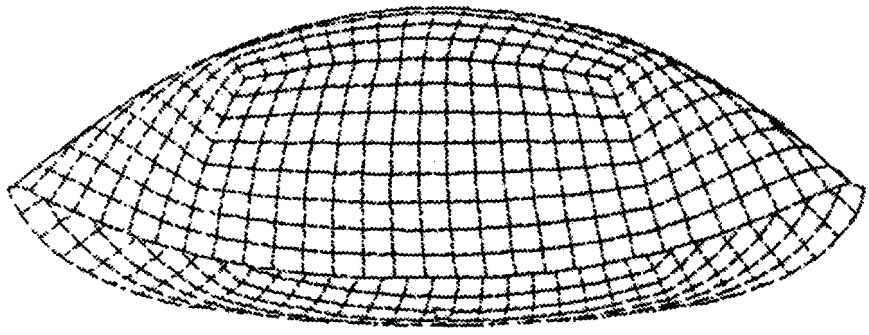

Fig. 13. Hemispherical shell: deformed shell.

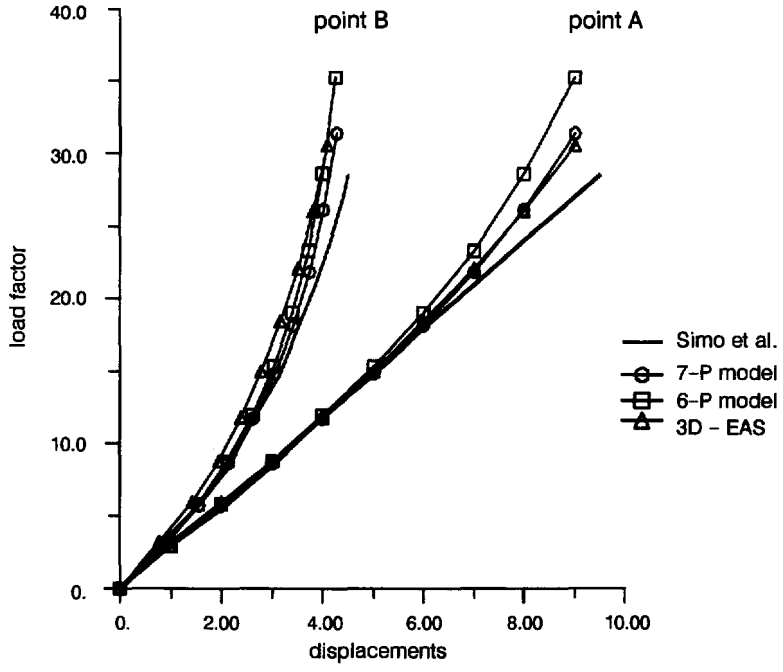

Fig. 14. Hemispherical shell: load–deflection diagram.

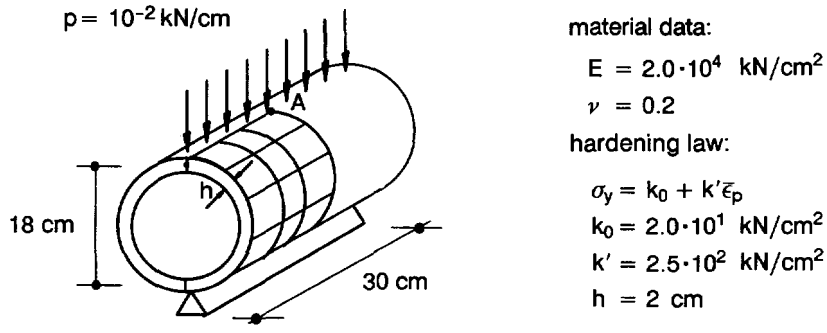

Fig. 15. Thick-walled cylindrical shell: data.

solution, whereas the six-parameter formulation is slightly too stiff. In addition, a solution of Simo *et al.* (1990) is added which resorts to a different material law defined in stress resultants. Therefore, the complete identification of the material parameter was difficult.

5.3. *Thick cylinder under line-load*

One quarter of the thick-walled cylindrical shell shown in Fig. 15 together with its data was idealized by a uniform 12×12 finite element mesh; the large deformation problem was

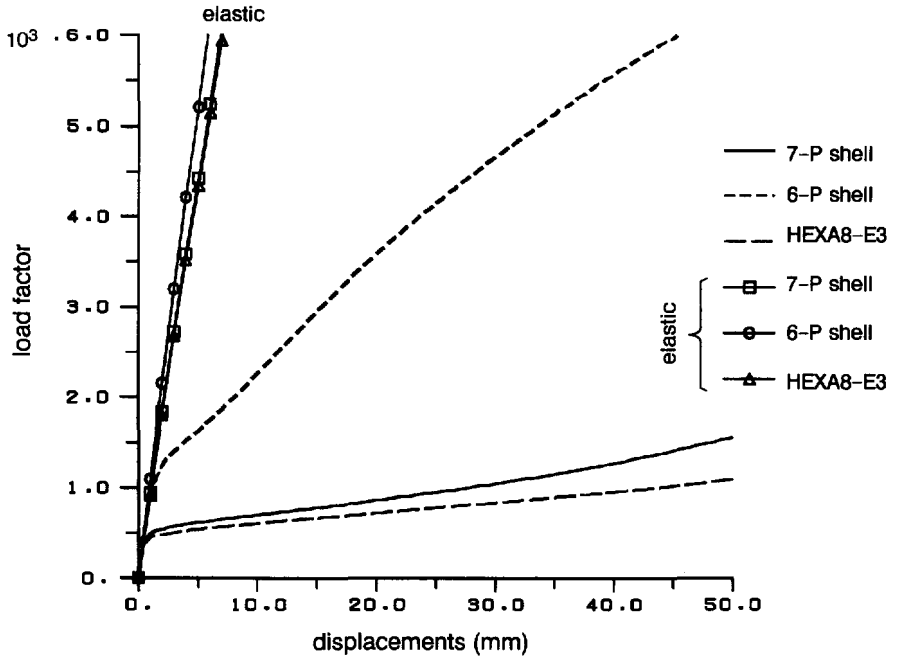

Fig. 16. Thick-walled cylindrical shell: load–deflection diagram.

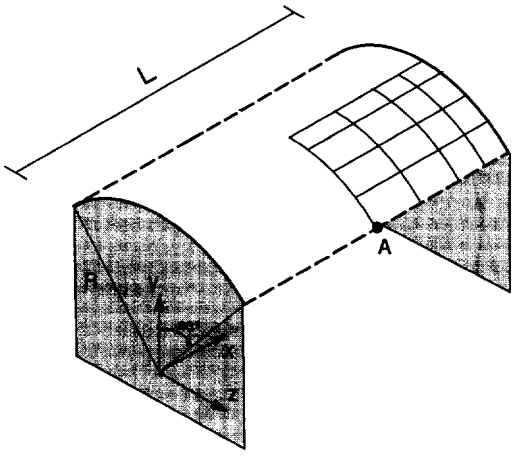

material data:
$E = 2.1 \cdot 10^4$ N/mm^2
$\nu = 0.0$
$\sigma_y = 4.2$ N/mm^2
(ideal plasticity)
geometry:
L = 15200 mm
h = 76 mm
R = 7600 mm
boundary conditions:
free
$U_y = U_z = 0$
dead load:
$q = 4.0 \cdot 10^{-3}$ N/mm^2

Fig. 17. Scordelis–Lo roof.

analyzed with an elastic and a large strain elasto-plastic material law. The six- and seven-parameter formulations are compared to the HEXA8-E3 continuum solution. The load deflection diagram for point A, Fig. 16, clearly indicates the "thickness locking" of the six-parameter solution.

5.4. *Shallow cylindrical shell*

The shallow cylindrical shell (Fig. 17) is a classical benchmark problem often referred to as "Scordelis–Lo roof"; 12×12 elements are used for one quarter of the structure.

The following models are compared:

—Five-parameter shell model with small strain plasticity, three, five or seven Simpson integration points (PSI) across the thickness and a condensed material law.
—Six- and seven-parameter shell model with large strain plasticity, with three or six Gauss integration points (GP) across the thickness and a complete three-dimensional material law.

The following models are compared:

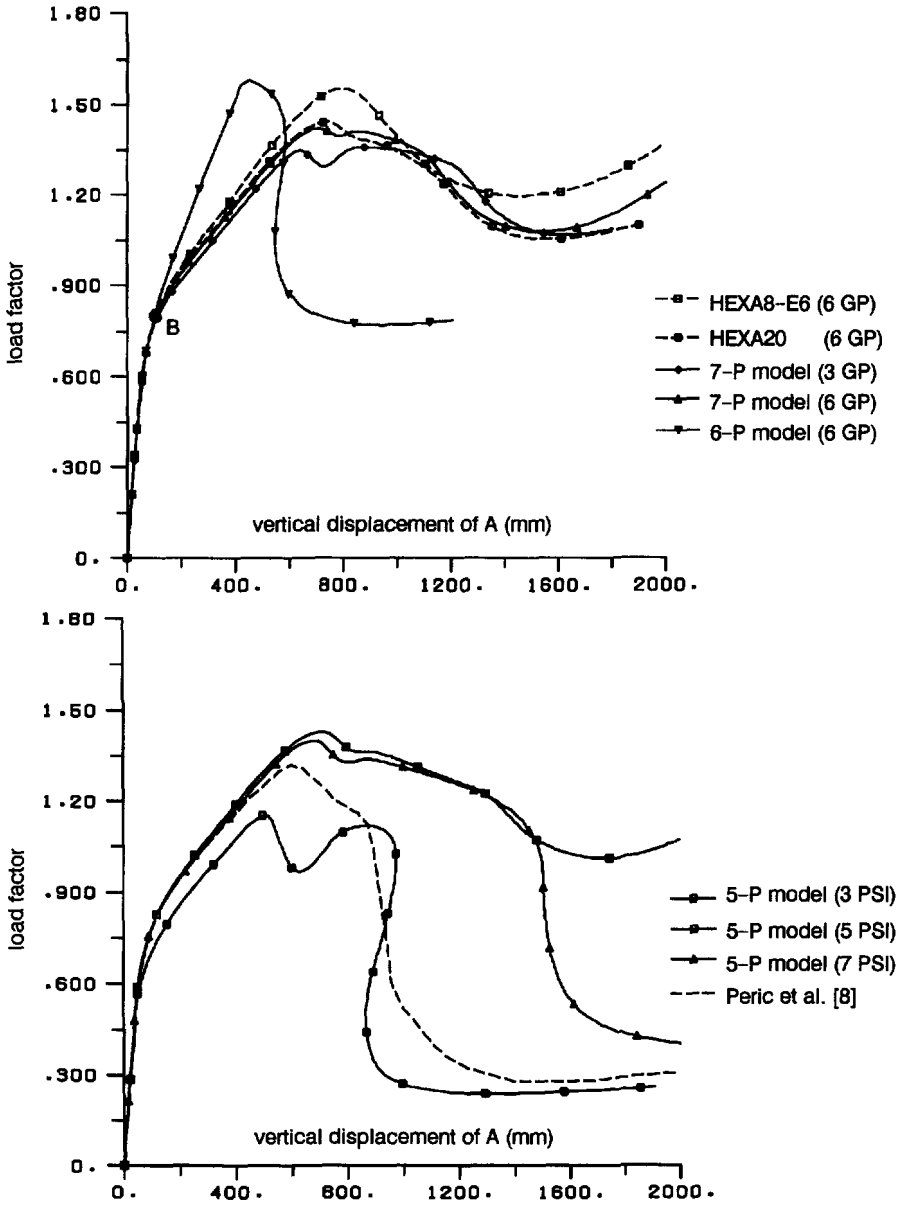

Fig. 18. Scordelis–Lo roof: load–deflection diagram for point A.

—Continuum solution with HEXA8-E6 elements and HEXA20 (20-node displacement model) with six Gauss integration points; two HEXA20 elements are chosen across the thickness, but only one HEXA8-E6.

—A reference solution by Peric and Owen (1991) who employed Morley triangular elements and large strain J_2-plasticity with a plane stress condition.

All models coincide in the low load range up to point B; see the load deflection diagrams in Fig. 18.

Then the solutions slightly deviate, although the seven-parameter model and the continuum models come very close independent of the chosen integration rule. Only the six-parameter solution is—as expected—too stiff. Although the five-parameter formulation has a similar tendency as the seven-parameter solution its results very much depend on the number of integration points. All solutions show at the beginning a failure mode with a kind of hinge at the top, mode 0 in Fig. 19. This mode is even more pronounced (mode 1) for the six-/seven-parameter and continuum solutions. The five-parameter solution finally

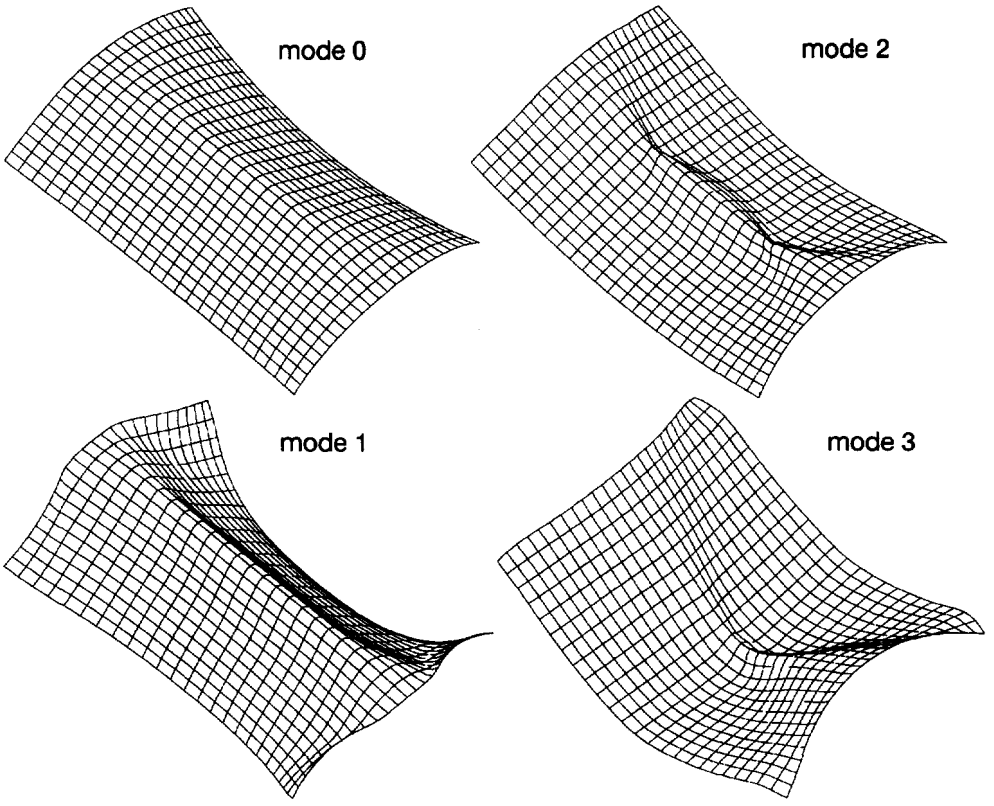

Fig. 19. Scordelis–Lo roof: failure modes.

ends up in mode 1 for 5 PSI, in mode 2 for 7 PSI and mode 3 for 3 PSI; the latter one is also indicated by the reference solution. This variety of solutions in the post-critical range is on purpose not suppressed in this study; it clearly demonstrates the large parameter sensitivity involved in this shell problem.

6. CONCLUSIONS

The study allows the following conclusions:

- The multiplicative elasto-plastic material model is well suited for the simulation of large deformations of solid structures; its algorithmic version is consistent and numerically efficient.
- The enrichment of the hexahedral eight-node brick element by three or six extra incompatible strain modes avoids volumetric locking due to a specific integration rule; no zero-energy modes are encountered. However, the numerical stability of these elements has to be further investigated. Since the hybrid concept returns to a pure displacement model the conventional strain driven material formulation can be preserved.
- The elements are also able to capture localization, such as shear bands. However, in order to avoid mesh dependency extra localization limiters and regularization schemes have to be introduced.
- The three-dimensional law can be directly introduced into a special large strain shell formulation; no reduction of the stress/strain field is necessary even for thin structures.

It is worth adding further features to the numerical model like thermal effects, kinematic hardening, combination with damage, contact, etc. This holds for the constitutive law, the enhanced assumed strain element and the application of the three-dimensional model to thin-walled structures like plates and shells.

Acknowledgement—The majority of this study has been strongly influenced by the work of Juan C. Simo. This valuable impact cannot be sufficiently enough appreciated. The financial support by a grant of the German Academic Exchange Council (DAAD) is also very much acknowledged.

REFERENCES

Andelfinger, U., Ramm, E. and Roehl, D. (1992). 2D and 3D enhanced assumed strain elements and their application in plasticity. In *Proceedings of the Conference on Computational Plasticity* (Edited by D. R. J. Owen, E. Hinton and E. Oñate). Pineridge Press, Barcelona.

Andelfinger, U. and Ramm, E. (1993). EAS-elements for two-dimensional, three-dimensional plate and shell structures and their equivalence to HR-elements. *Int. J. Num. Meth. Eng.* **36,** 1311–1337.

Büchter, N. and Ramm, E. (1992). 3D-extension of nonlinear shell equations based on the enhanced assumed strain concept. In *Proceedings of European Conference on Numerical Methods in Engineering* (Edited by C. Hirsch *et al.*), pp. 55–62. Elsevier, Brussels.

Büchter, N., Ramm, E. and Roehl, D. (1994). Three-dimensional extension of nonlinear shell formulation based on the enhanced assumed strain concept. *Int. J. Num. Meth. Eng.* **37,** 2551–2568.

Irons, B. M. (1971). Quadrature rules for brick based finite elements. *Int. J. Num. Meth. Eng.* **3,** 293–294.

Lee, E. H. (1969). Elastic–plastic deformation at finite strains. *J. Appl. Mech.* **36,** 1–6.

Nadai, A. (1950). *Theory of Flow and Fracture of Solids*, Vol. 1. MacGraw-Hill.

Peric, D. and Owen, D. R. J. (1991). The Morley thin shell finite element for large deformation problems: simplicity versus sophistication. In *Nonlinear Engineering Computations* (Edited by N. Bicanic *et al.*). Pineridge Press, Swansea.

Reddy, B. D. and Simo, J. C. (1992). Stability and convergence of a class of enhanced strain methods. FRD/UCT Center for Research in Computational and Applied Mechanics, Report No. 174, University of Cape Town, South Africa.

Roehl, D. (1994). Zur Berechnung von groen elasto-plastischen Deformationen bei Flächentragwerken und Kontinua. Ph.D.—Dissertation, Bericht Nr. 16, Institut für Baustatik, Universität Stuttgart.

Simo, J. C. and Armero, F. (1992). Geometrically non-linear enhanced strain mixed methods and the method of incompatible modes. *Int. J. Num. Meth. Eng.* **33,** 1413–1449.

Simo, J. C. and Rifai, M. S. (1990). A class of assumed strain methods and the method of incompatible modes. *Int. J. Num. Meth. Eng.* **29,** 1595–1638.

Simo, J. C. (1988a). A framework for finite strain elastoplasticity based on maximum plastic dissipation and the multiplicative decomposition: Part I. Continuum formulation. *Comp. Meth. Appl. Mech. Eng.* **66,** 199–219.

Simo, J. C. (1988b). A framework for finite strain elastoplasticity based on maximum plastic dissipation and the multiplicative decomposition: Part II. Computational aspects. *Comp. Meth. Appl. Mech. Eng.* **68,** 1–31.

Simo, J. C. and Taylor, R. L. (1985). Consistent tangent operators for rate-independent elasto-plasticity. *Comp. Meth. Appl. Mech. Eng.* **48,** 101–118.

Simo, J. C., Rifai, M. S. and Fox, D. D. (1990). On a stress resultant geometrically exact shell model, Part IV: variable thickness shells with through-the-thickness stretching. *Comp. Meth. Appl. Mech. Eng.* **81,** 53–91.

Simo, J. C., Armero, F. and Taylor, R. L. (1993). Improved versions of assumed enhanced-strain tri-linear elements for 3D finite deformation problems. *Comp. Meth. Applied Mech. Eng.* **110,** 359–386.

Taylor, R. L., Simo, J. C., Zienkiewicz, O. C. and Chan, A. C. (1986). The Patch-test: a condition for assessing finite element convergence. *Int. J. Num. Meth. Eng.* **22,** 39–62.

Wilkins, M. L. (1964). Calculation of elasto-elastic flow. In *Method of Computational Physics* 3 (Edited by B. Alder *et al.*). Academic Press, New York.

APPENDIX A

A.1. Element matrices

The element stiffness matrix is decomposed into its material and its geometrical part:

$$\mathbf{k}^e(\mathbf{d}^e, \boldsymbol{\alpha}^e) = \begin{bmatrix} k_{11} & k_{12} \\ k_{21} & k_{22} \end{bmatrix}^e = \mathbf{k}_M^e + \mathbf{k}_G^e \tag{A1}$$

with $k_{ij} = k_{Mij} + k_{Gij}$ according to eqn (50):

$$\mathbf{k}_{M11} = \int_{B_{0_e}} \mathbf{B}^T J \mathbb{C} \mathbf{B} \, dV \qquad \mathbf{k}_{G11} = \int_{B_{0_e}} \mathbf{B}_T^G \tilde{\boldsymbol{\tau}} \mathbf{B}_G \, dV$$

$$\mathbf{k}_{M22} = \int_{B_{0_e}} \tilde{\mathbf{B}}^T J \mathbb{C} \tilde{\mathbf{B}} \, dV \qquad \mathbf{k}_{G22} = \int_{B_{0_e}} \tilde{\mathbf{B}}_G^T \tilde{\boldsymbol{\tau}} \tilde{\mathbf{B}}_G \, dV$$

$$\mathbf{k}_{M12} = \mathbf{k}_{M21}^T = \int_{B_{0_e}} \mathbf{B}^T J \mathbb{C} \tilde{\mathbf{B}} \, dV \quad \mathbf{k}_{G12} = \mathbf{k}_{G21}^T = \int_{B_{0_e}} \mathbf{B}_G^T \tilde{\boldsymbol{\tau}} \tilde{\mathbf{B}}_G \, dV. \tag{A2}$$

The indices 1 and 2 refer to the nodal displacement parameter $\mathbf{d}^e$ and the internal unknowns $\boldsymbol{\alpha}^e$, respectively. Similarly the vector of the internal forces is decomposed:

$$\mathbf{f}_1 = \int_{B_0} \mathbf{B}^T \bar{\boldsymbol{\tau}} \, dV \quad \text{and} \quad \mathbf{f}_2 = \int_{B_0} \bar{\mathbf{B}}^T \bar{\boldsymbol{\tau}} \, dV. \tag{A3}$$

A.2. Nonlinear solution strategy with EAS concept

(a) On element level:

a1. update of nodel displacements:

$$\mathbf{d}^{(K+1)} = \mathbf{d}^{(K)} + \Delta\mathbf{d}^{(K)} \tag{A4}$$

a2. update of extra element variables:

$$\Delta\boldsymbol{\alpha}^{e(K)} = -[\mathbf{k}_{22}^{-1}(\mathbf{f}_2 + \mathbf{k}_{21}\,\Delta\mathbf{d}^e)]^{(K)} \tag{A5}$$

$\longrightarrow$ have to be stored

and

$$\boldsymbol{\alpha}^{e(K+1)} = \boldsymbol{\alpha}^{e(K)} + \Delta\boldsymbol{\alpha}^{e(K)}. \tag{A6}$$

(b) At integration point:

b1. calculation of enhanced deformation gradient:

$$\tilde{\mathbf{F}}^h = \mathbf{F}^h + \tilde{\mathbf{H}}^h = \sum_{K=1}^{NK} \mathbf{x}_K^e(t) \cdot \mathrm{Grad}[\mathbf{N}^K] + \sum_{I=1}^{N\alpha} \alpha_I^e \mathbf{G}_e^I \tag{A7}$$

b2. calculation of strains and stress predictor,

b3. application of projection algorithm,

b4. integration of element matrices and internal force vector (residium).

a3. condensation of extra element variables $\boldsymbol{\alpha}^e$:

$$\tilde{\mathbf{k}}^e = [\mathbf{k}_{11} - \mathbf{k}_{21}^T \mathbf{k}_{22}^{-1} \mathbf{k}_{12}]$$

$$\tilde{\mathbf{r}}^e = [\mathbf{f}^u - \mathbf{f}_1 + \mathbf{k}_{12}^T \mathbf{k}_{22}^{-1} \mathbf{f}_2]. \tag{A8}$$

(c) On structural level:

c1. assembly of structural matrices ($\mathbf{A}$ = assembly operator):

$$\tilde{\mathbf{K}} = \mathop{\mathbf{A}}_{e=1}^{ne} \tilde{\mathbf{k}}^e$$

$$\tilde{\mathbf{R}} = \mathop{\mathbf{A}}_{e=1}^{ne} \tilde{\mathbf{r}}^e \tag{A9}$$

c2. solution for new displacement increment:

$$\Delta\mathbf{d}^{K+1} = [\tilde{\mathbf{K}}^{(K+1)}]^{-1} \tilde{\mathbf{R}}^{K+1} \tag{A10}$$

c3. convergence check $\nearrow$ yes $\Rightarrow$ next loadstep

$\searrow$ no $\Rightarrow$ $k \leftarrow k+1$, go to (a).